PHYSICAL REVIEW B **96**, 144437 (2017)

Effects of cobalt substitution in $L1_0$ -(Fe,Co)Pt thin films

Shoya Sakamoto,[1] Kumar Srinivasan,[2] Rui Zhang,[2,*] Oleg Krupin,[2,*] Keisuke Ikeda,[1] Goro Shibata,[1] Yosuke Nonaka,[1]
Zhendong Chi,[1] Masako Sakamaki,[3] Kenta Amemiya,[3] Atsushi Fujimori,[1] and Antony Ajan[2]
[1]*Department of Physics, The University of Tokyo, 7-3-1 Hongo, Bunkyo-ku, Tokyo 113-0033, Japan*
[2]*Western Digital, 1710 Automation Parkway, San Jose, California 95131, USA*
[3]*Institute of Materials Structure Science, High Energy Accelerator Research Organization, 1-1 Oho, Tsukuba, Ibaraki 305-0801, Japan*

(Received 23 August 2017; published 30 October 2017)

We have studied the effect of cobalt substitution in $L1_0$-$Fe_{1-x}Co_xPt$ films by means of x-ray magnetic circular dichroism (XMCD) and first-principles calculations. The magnetic moments of Fe ($\sim$2.5 μ_B) and Co ($\sim$1.5 μ_B) deduced using XMCD were almost unchanged upon Co doping, and the net magnetization decreases with increasing Co content. Calculation also showed that the $3d$ electrons that have been added by Co substitution occupy only spin-down bands.

DOI: 10.1103/PhysRevB.96.144437

Owing to the development of information technology, the overall amount of information has been increasing explosively. In such circumstances, hard disk drives (HDDs) have played a central role as storage devices, where the assembly of ferromagnetic grains is used as a bit. To achieve even higher areal bit density by decreasing the size of the grains, it is necessary to use materials with large magnetic anisotropy so that the decrease of the grain volume V is compensated by the increase of the magnetic anisotropy energy K, maintaining the thermal stabilization factor KV/k_BT large enough, say above 60 [1]. $L1_0$-ordered FePt and CoPt are promising materials since they possess very large K of 7.0×10^7 erg/cm^3 and 4.9×10^7 erg/cm^3, respectively [2,3]. To utilize these materials as a media for HDDs, a large value of saturation magnetization M_S is also required to increase the signal level and to achieve an adequate signal-to-noise ratio (SNR). The reported M_S values of $L1_0$ FePt and CoPt are about 1100 emu/cm^3 [3–5] and 800 emu/cm^3 [3,6], respectively, at room temperature.

In previous studies employing macroscopic magnetometry such as superconducting quantum interference device (SQUID) or vibrating sample magnetometer (VSM) measurements, mixed compounds $Fe_{1-x}Co_xPt$ were reported to have larger net magnetization than pristine FePt, which would be a promising property for future HDD applications. A 14% increase was observed for $(Fe_{0.5}Co_{0.5})_{60.5}Pt_{39.5}$ bulk specimen [7], 15% for $(Fe_{0.85}Co_{0.15})_{50}Pt_{50}$ thin film [8], and even 54% for $(Fe_{0.8}Co_{0.2})_{59}Pt_{41}$ thin film [9]. However, first-principles calculations [10,11] suggested that the net magnetization decreases with increasing Co content.

In order to resolve this issue, we have performed x-ray absorption spectroscopy (XAS) and x-ray magnetic circular dichroism (XMCD) measurements, by which one can obtain the (effective) spin and orbital magnetic moments of each constituent element separately [12–14]. Since XAS and XMCD are also sensitive to chemical states [15], it is possible to deduce the intrinsic magnetic moments excluding contributions from impurities such as surface oxides [16,17]. In addition, we have done first-principles calculations to deduce the magnetic dipole term in the spin sum rule and to discuss the effect of Co substitution in FePt films.

Samples were grown using the dc and rf sputtering methods on glass substrates. The sample structure was “C cap (4 nm)/$Fe_{1-x}Co_xPt$ (22 nm)/MgO (20 nm)/seed/glass substrate” ($x = 0$, 0.05, 0.1, 0.15, 0.3). Because we found strong oxide peaks in the XAS spectrum of the $x = 0$ sample, we used another sample with the different structure of “C cap (4 nm)/FePt (5 nm)/MgO (5 nm)/seed/glass substrate” for XAS and XMCD measurements. The MgO, C layers were grown at room temperature, while the $Fe_{1-x}Co_xPt$ layer was grown at the elevated temperature of 600 °C to achieve the (001)-oriented $L1_0$-ordered phase [18]. We used separate Fe, Co, and Pt targets to control the composition.

XAS and XMCD measurements were conducted at beamline BL-16A1 of the Photon Factory (PF), High Energy Accelerator Research Organization (KEK). The spectra were taken at room temperature in the total-electron-yield (TEY) mode. A magnetic field of 5 T was applied parallel to the incident x rays and perpendicular to the film surface so that the magnetization of $Fe_{1-x}Co_xPt$ was fully saturated. A double-step function with amplitude ratio 2:1 representing the L_3- and L_2-edge jumps were subtracted from each absorption spectrum [19].

First-principles calculations with the local-density approximation (LDA) were performed using a WIEN2K package. Spin-orbit interaction was also included. In order to study the effect of Co substitution, we constructed supercells containing Co atoms at the Fe sites as shown in the Supplemental Material [20]. We assumed Vegard’s relation of $a = 3.863(1 - x) + 3.806x$ and $c = 3.710(1 - x) + 3.684x$ for the lattice constants of $Fe_{1-x}Co_xPt$ [21,22].

Figure 1 shows the XAS spectra of $Fe_{1-x}Co_xPt$ recorded at the Fe and Co $L_{2,3}$ absorption edges, where they have been normalized to unity at the peak of the L_3 absorption edge for each element. The Fe XAS spectra show a shoulder at around $\sim$710 eV, which did not in the previous studies of FePt films [23,25]. This can be attributed to signals from Fe oxides formed at the surface because the position of the shoulder corresponds to the peak position of the XAS spectra of Fe^{3+} compounds such as Fe_2O_3 [25], and because the intensities of the shoulder showed nonmonotonic behavior as a function of Co content. Such shoulders were not seen in the Co XAS spectra, where

---

[*] Contributed during a stay at Western Digital.

2469-9950/2017/96(14)/144437(5)

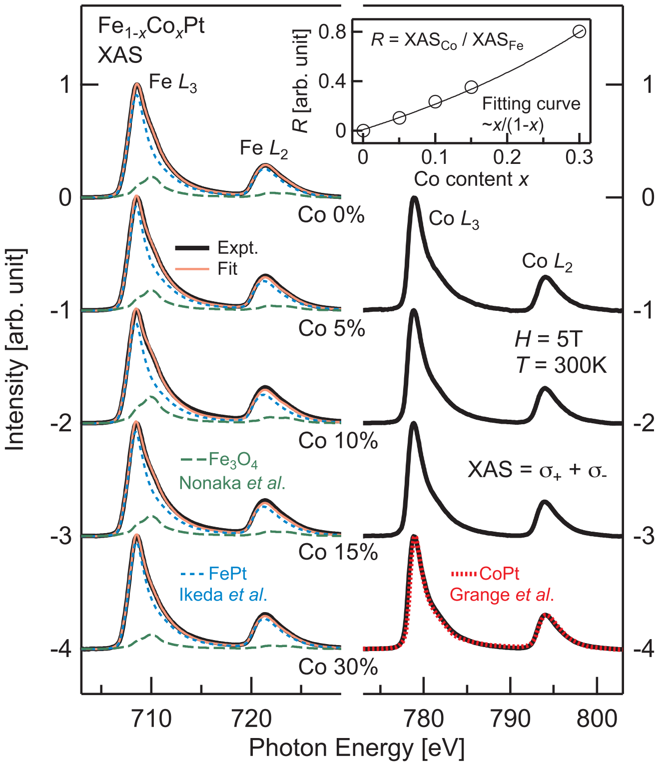

FIG. 1. Fe and Co $L_{2,3}$-edge XAS spectra of Fe$_{1-x}$Co$_x$Pt. The Fe XAS spectra were fitted by the summation of FePt [23] (blue dashed) and Fe$_3$O$_4$ (green dashed) [24] spectra. The fitted results are shown by pink solid curves. The XAS spectrum of $L1_0$-CoPt [6] is also shown by a red dashed curve as a reference. The inset shows the ratio R of Co $L_{2,3}$ XAS integral to the Fe one as a function of Co content x.

the spectral line shape did not change upon Co doping. This can be naturally understood because Co is more difficult to be oxidized than Fe. Since the Fe XAS spectra contain signals from surface oxides, we have decomposed the spectra into FePt [23] and Fe oxide components by least-squares fitting. Here, we have used the Fe$_3$O$_4$ spectrum [24] in order to reflect the contributions from both Fe^{2+} and Fe^{3+} oxides. Note that the following discussion would not be affected if we adopt the Fe$_2$O$_3$ spectrum, but a fit using the Fe$_3$O$_4$ better reproduced the experimental spectra, as was also mentioned in Ref. [25]. The fitted results are shown by pink solid curves, and the FePt and Fe$_3$O$_4$ spectrum components are also separately shown by blue and green dashed curves, respectively. This decomposition is crucial when estimating the magnetic moments using XMCD sum rules [12,13].

The inset of Fig. 1 shows the ratio of the XAS area of Co to that of Fe as a function of Co content x. The data are well fitted to $Ax/(1-x)$, where A is a proportionality constant. This confirms that the actual concentration of Fe and Co atoms, or at least its ratio, is very close to the designed values.

Figure 2 shows the XMCD spectra of Fe$_{1-x}$Co$_x$Pt. They are nearly identical to those of FePt [23] and CoPt [6], as shown by blue and red dashed curves, respectively. This indicates that the local electronic structure of the Fe$_{1-x}$Co$_x$Pt alloy is similar to their two end members FePt and CoPt. Note that the Fe-oxide shoulder seen in the XAS spectra was absent in the XMCD spectra, presumably because naturally formed Fe oxides are usually nonferromagnetic.

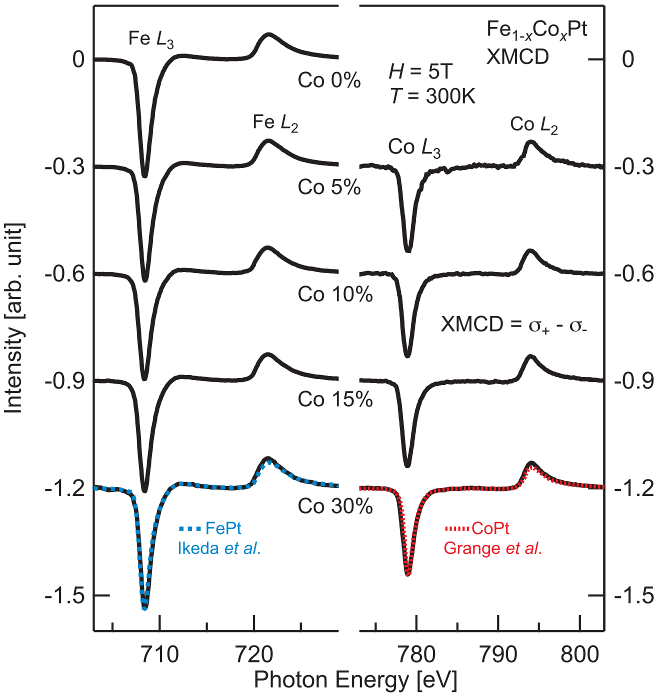

FIG. 2. XMCD spectra of Fe$_{1-x}$Co$_x$Pt at Fe and Co $L_{2,3}$ edges. The spectra of $L1_0$-ordered FePt and CoPt are shown as references by blue and red dashed curves, respectively.

We have estimated the spin and orbital magnetic moments of Fe and Co by applying the XMCD sum rules [19]:

$$m_l = -\frac{4\int_{L_{2,3}} \sigma_+ - \sigma_-\, d\omega}{3\int_{L_{2,3}} \sigma_+ + \sigma_-\, d\omega} n_h, \tag{1}$$

$$m_s^{\mathrm{eff}} = -\frac{2\int_{L_3} \sigma_+ - \sigma_-\, d\omega - 4\int_{L_2} \sigma_+ - \sigma_-\, d\omega}{\int_{L_{2,3}} \sigma_+ + \sigma_-\, d\omega} n_h, \tag{2}$$

$$m_s^{\mathrm{eff}} = m_s + 7m_T, \tag{3}$$

where σ_+ and σ_- denote absorption cross sections, namely, XAS intensity, measured with x rays with positive and negative helicity. m_l and m_s are the orbital and spin magnetic moments, m_s^{eff} the effective spin magnetic moment, and m_T the magnetic dipole term in units of μ_B/atom. Note that each term can be written as $m_s = -2\mu_B\langle S_\alpha\rangle/\hbar$, $m_l = -\mu_B\langle L_\alpha\rangle/\hbar$, and $m_T = -\mu_B\langle T_\alpha\rangle/\hbar$, where $\boldsymbol{S}$ denotes the spin angular momentum operator, $\boldsymbol{L}$ the orbital angular momentum operator, $\boldsymbol{T}$ the magnetic dipole operater $\boldsymbol{T} = \boldsymbol{S} - 3\hat{r}(\hat{r}\cdot\boldsymbol{S})$, and α represents the incident x-ray direction [26]. The number of holes in the Fe and Co $3d$ shell, denoted by n_h, was assumed to be 3.4 and 2.63, respectively [6,25]. As for the Fe XAS area, which appears in the denominators of Eqs. (1) and (2), we used the fitted FePt component to exclude oxide contributions. By applying this correction, the estimated magnetic moments increased by at most ~30%.

Although the m_T term can be ignored in cubic systems with T_d or O_h symmetry, it cannot be neglected in the case of highly anisotropic systems such as $L1_0$-ordered alloys. Here we estimate the m_T of Fe (Co) atom in FePt (CoPt) as follows.

TABLE I. Orbital and (effective) spin magnetic moments of Fe and Co in $\mathrm{Fe}_{1-x}\mathrm{Co}_x\mathrm{Pt}$. m_l and m_s denote the orbital and spin magnetic moments, respectively, and $m_s^{\mathrm{eff}} = m_s + 7m_T$ the effective spin magnetic moment, where m_T is the magnetic dipole term. m_{Fe} and m_{Co} represent the summation of the orbital and spin magnetic moments for each atom, where the m_T term has been subtracted as described in the main text. m_{net} [$=(1-x)m_{\mathrm{Fe}} + xm_{\mathrm{Co}}$] represents the net magnetic moment and M_{net} the net magnetization of the film in units of emu/cm^3 taking the Pt magnetic moments of $0.38(1-x) + 0.42x$ μ_{B} into account. Note that uncertainties are shown in parentheses.

	Fe [μ_{B}]				Co [μ_{B}]				m_{net}	M_{net}
$\mathrm{Fe}_{1-x}\mathrm{Co}_x\mathrm{Pt}$	m_l	$m_s + 7m_T$	m_l/m_s^{eff}	m_{Fe}	m_l	$m_s + 7m_T$	m_l/m_s^{eff}	m_{Co}	[μ_{B}]	[emu/cm^3]
$x = 0$	0.27(3)	2.07(10)	0.13(2)	2.49(11)					2.49(11)	961
0.05	0.25(3)	2.06(10)	0.12(1)	2.47(11)	0.22(4)	1.25(13)	0.17(3)	1.45(13)	2.42(10)	942
0.10	0.19(2)	2.04(10)	0.10(1)	2.39(10)	0.23(4)	1.12(12)	0.20(4)	1.33(11)	2.28(9)	896
0.15	0.20(2)	2.02(10)	0.10(1)	2.36(10)	0.22(4)	1.27(13)	0.17(3)	1.46(12)	2.23(9)	881
0.30	0.20(2)	2.12(11)	0.10(1)	2.45(11)	0.17(3)	1.31(14)	0.13(3)	1.47(12)	2.15(8)	863
0 (Expt. [25])	0.19	2.21	0.09	2.40[a]					2.40[a]	931[a]
0 (LSDA)	0.072	2.87 -0.25	0.025	2.94					2.94	1110
1 (Expt. [6])					0.26	1.76	0.148	2.02[a]	2.02[a]	840[a]
1 (LSDA)					0.109	1.79 0.033	0.061	1.90	1.90	806
0-1 (CPA[10])				2.9				1.8	$2.9 - 1.1x$	

[a] Effective values containing the $7m_T$ term.

When spin-orbit coupling is weak and charge and spin are decoupled as in $3d$ transition metals, m_T can be expressed as [26]

$$7m_T \approx \sum_i \frac{7}{2} Q_\alpha^i m_s^i = \sum_i \frac{7}{2} Q_\alpha^i \Delta n_i \mu_{\mathrm{B}}, \tag{4}$$

$$Q_\alpha^i = \langle d_i | Q_{\alpha\alpha} | d_i \rangle, \quad Q_{\alpha\beta} = \delta_{\alpha\beta} - 3r_\alpha r_\beta / r^2, \tag{5}$$

where $\alpha,\beta = x,y$, or z denotes the Cartesian frame. m_s^i is the spin magnetic moment of electrons in a d_i orbital, which is directly related to Δn_i ($=n_{i,\uparrow} - n_{i,\downarrow}$) the difference between occupation numbers of spin-up and spin-down electrons in the orbital. The values of Q_α^i are summarized in Ref. [26], and Δn_i can be easily calculated by first-principles calculation. In the out-of-plane geometry, $7m_T$ of FePt and CoPt were calculated to be -0.246 μ_{B} and 0.0326 μ_{B}, respectively, while in the in-plane geometry, 0.123 μ_{B} and -0.0171 μ_{B} [27]. These values agree with the sum rules applications to the calculated XMCD spectra by first-principles calculations [28]. Therefore, one should be careful about the spin magnetic moment of Fe in FePt with a high degree of $L1_0$ order, where $m_s^{\mathrm{eff}} = m_s + 7m_T$ may be smaller than m_s by at most ∼15%. Note that we could confirm that this simple calculation reproduced the reported values of m_T of CrO_2 [29].

The obtained effective spin and orbital moments are summarized in Table I together with the previous experimental and theoretical results. The obtained spin magnetic moments of Fe are similar to the previous experimental study [25], but those of Co are smaller than the results of Ref. [6]. This is probably because some of the Co atoms are magnetically inactive near the surface with oxidized Fe. In fact, if the area ratios of the raw Fe XAS spectra to the fitted FePt components are also multiplied to the Co magnetic moments, the values become as large as those in Ref. [6].

Figure 3(a) shows the magnetic moments $m_s + m_l$ of Fe taking the oxides component and m_T term into account. Although the raw data (black diamonds) showed nonmonotonic behavior, the moments became almost constant after the subtraction of the oxides component from the raw XAS spectra, as shown by the orange squares. Further, the subtraction of the m_T term had a minor effect on how the magnetic moments behave with Co content, as shown by the blue circles. Here, the $7m_T$ term was most simply estimated as $(7m_T/m_s)^{\mathrm{calc}} m_s^{\mathrm{expt}} S$ by assuming a linear relationship between m_T and the degree of $L1_0$ order S. S was deduced from the intensity ratio of the superlattice peak $I(110)$ to the fundamental peak $I(200)$ in the in-plane XRD profiles [30] as $S^2 = \frac{[I(110)/I(200)]^{\mathrm{obs}}}{[I(110)/I(200)]^{\mathrm{theor}}}$ [31] and is plotted in Fig. 3(c). Note that the m_T term for Co is negligibly small according to our LDA calculation.

Figure 3(b) summarizes the corrected magnetic moments of Fe and Co and the net magnetic moments of $\mathrm{Fe}_{1-x}\mathrm{Co}_x\mathrm{Pt}$. Since both the Fe and Co magnetic moments were almost constant as functions of Co content, the net magnetic moment was found

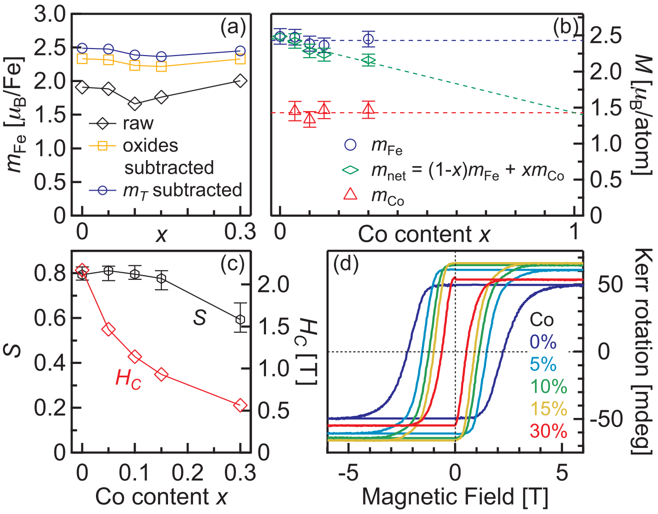

FIG. 3. (a) Magnetic moments of Fe before and after the corrections. (b) Magnetic moments of Fe and Co, and the net magnetic moment of $\mathrm{Fe}_{1-x}\mathrm{Co}_x\mathrm{Pt}$ as a function of Co content. (c) Degree of $L1_0$ order and coercive field. (d) Out-of-plane magnetic hysteresis measured by the magneto-optical Kerr effect.

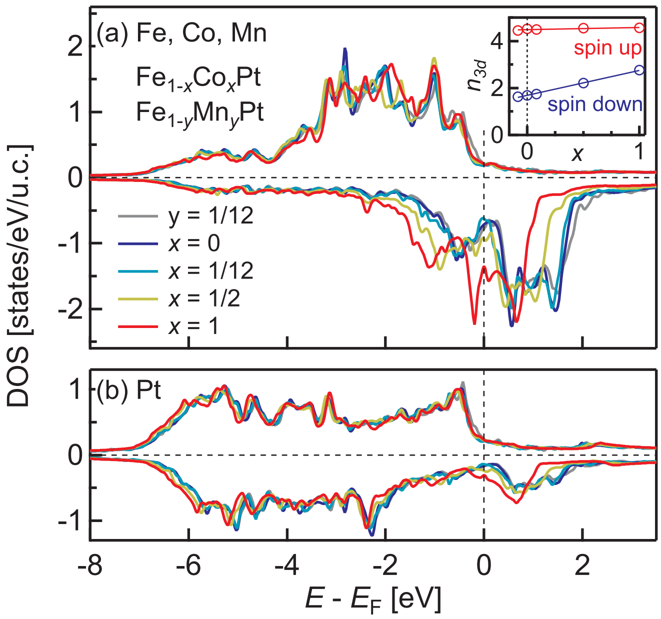

FIG. 4. Densities of states (DOSs) of $Fe_{1-x}Co_xPt$ and $Fe_{1-y}Mn_yPt$. The partial DOSs of the 3*d* transition metals and Pt are separately shown in panels (a) and (b). Inset shows the 3*d* orbital occupation number for each of the spin-up and spin-down bands.

to decrease with Co doping. This disagrees with the previous experiments [7–9] but agrees with the theoretical prediction [10]. In Fig. 3(b), blue and red solid lines represent averaged values of the magnetic moment of Fe and Co, respectively, and the green line values calculated from them. Fitting using a linear function also reproduced the blue and green lines, although fitting to the Co magnetic moment showed slightly increasing behavior due to the fewer data points. Note that the Pt magnetic moments, which can be as large as 0.38–0.42 μ_B [28], have not been considered.

Out-of-plane magnetic hysteresis curves were also measured by the magneto-optical Kerr effect (MOKE) and are shown in Fig. 3(d). The coercive field (H_C) is also plotted in Fig. 3(c). In spite of the small change in the degree of $L1_0$ order caused by Co substitution, H_C or the magnetic anisotropy decreases rather rapidly.

In order to understand the microscopic mechanism as to why the magnetization decreased with Co doping, we have calculated the densities of states (DOSs) of $Fe_{1-x}Co_xPt$. Figure 4(a) shows the Fe and Co partial DOS for the varying Co content. The DOSs of spin-up bands are almost fully occupied and unchanged upon doping, while those of spin-down bands shift upward without a significant change in the line shapes, and concomitantly their occupation number increases. This suggests that the Co substitution does not change the band structure significantly but simply provides the spin-down bands with electrons. The inset shows the electron occupation numbers of the spin-up and spin-down 3*d* bands (n_{3d}). The spin-up bands are almost completely filled with 4.5 electrons and the occupation number is nearly constant with Co content. On the other hand, the occupation number of the spin-down bands shows a linear increase. This can be understood because Co has one more 3*d* electron than Fe, and further electron doping leads to the occupation of spin-down bands. Note that the Pt partial DOS showed little change as shown in Fig. 4(b), and the occupation number of Pt 5*d* orbitals was almost unchanged.

To summarize, the XMCD results have clarified that the net magnetic moment of $Fe_{1-x}Co_xPt$ decreases with increasing Co content because the additional electron provided by Co occupies the spin-down bands instead of the almost completely filled spin-up bands. The discrepancy between the present results and the previous experiments [7–9] would be attributed to some experimental artefacts such as errors in estimating the volume of FePt. Especially in the case of granular thin films, it is difficult to estimate the film thickness and the packing density of grains with sufficient accuracy. The present results also indicate that the magnetic moment may increase when holes are doped to the system. To elaborate this conjecture, we have also calculated the DOS of Mn-substituted FePt. The spin-down DOS indeed shows a shift to the opposite direction, i.e., upward as expected. The occupation number is also plotted in the inset at the position of $x = -1/12$, representing a hole doping, and extrapolates from the trend of electron doping by Co. Therefore, the small amount of hole doping by Mn substitution or some other methods might be a better way to improve the magnetic properties of FePt. Actually, the effect of band filling [32,33] and Mn substitution [34] on the magnetic properties of FePt were theoretically studied, and it was reported that the magnetic anisotropy as well as magnetization can be enhanced. However, too much doping may not be effective [35] because $L1_0$-MnPt is antiferromagnetic.

This work was supported by Grants-in-Aid for Scientific Research from the JSPS (Grants No. 15H02109 and No. 15K17696). The experiment was done under the approval of the Photon Factory Program Advisory Committee (Proposals No. 2013S2-004, No. 2016S2-005, and No. 2016G006). Part of this work was conducted at Advanced Characterization Nanotechnology Platform of the University of Tokyo, supported by "Nanotechnology Platform" of MEXT, Japan. S.S. acknowledges financial support from the Advanced Leading Graduate Course for Photon Science (ALPS) and the JSPS Research Fellowship for Young Scientists. This collaboration was initiated when S.S. was doing an internship at Western Digital under the ALPS program. Z.C. acknowledges financial support from the Materials Education Program for Future Leaders in Research, Industry and Technology (MERIT). A.F. is an adjunct member of the Center for Spintronics Research Network (CSRN), the University of Tokyo, under the Spintronics Research Network of Japan (Spin-RNJ).

---

[1] S. H. Charap, P.-L. Lu, and Y. He, IEEE Trans. Magn. **33**, 978 (1997).

[2] M. Kryder, E. Gage, T. McDaniel, W. Challener, R. Rottmayer, G. Ju, Y.-T. Hsia, and M. Erden, Proc. IEEE **96**, 1810 (2008).

[3] D. Weller, O. Mosendz, G. Parker, S. Pisana, and T. S. Santos, Phys. Status Solidi A **210**, 1245 (2013).

[4] S. Okamoto, N. Kikuchi, O. Kitakami, T. Miyazaki, Y. Shimada, and K. Fukamichi, Phys. Rev. B **66**, 024413 (2002).

[5] T. Bublat and D. Goll, J. Appl. Phys. **108**, 113910 (2010).

[6] W. Grange, I. Galanakis, M. Alouani, M. Maret, J.-P. Kappler, and A. Rogalev, Phys. Rev. B **62**, 1157 (2000).

[7] S. Saha, C. J. Thong, M. Q. Huang, R. T. Obermyer, B. J. Zande, V. K. Chandhok, S. Simizu, and S. G. Sankar, J. Appl. Phys. **91**, 8810 (2002).

[8] Y. Liu and D. Sellmyer, IEEE Trans. Magn. **49**, 3292 (2013).

[9] Y. Lai, Y. Chang, Y. Chen, H.-J. Lin, and G. Chen, J. Mater. Sci. **42**, 6887 (2007).

[10] J. Maclaren, S. Willoughby, M. McHenry, B. Ramalingam, and S. Sankar, IEEE Trans. Magn. **37**, 1277 (2001).

[11] R. Cuadrado, T. J. Klemmer, and R. W. Chantrell, Appl. Phys. Lett. **105**, 152406 (2014).

[12] P. Carra, B. T. Thole, M. Altarelli, and X. Wang, Phys. Rev. Lett. **70**, 694 (1993).

[13] B. T. Thole, P. Carra, F. Sette, and G. van der Laan, Phys. Rev. Lett. **68**, 1943 (1992).

[14] J. Stöhr, J. Electron Spectrosc. Relat. Phenom. **75**, 253 (1995).

[15] F. de Groot, J. Electron Spectrosc. Relat. Phenom. **67**, 529 (1994).

[16] Y. Takeda, M. Kobayashi, T. Okane, T. Ohkochi, J. Okamoto, Y. Saitoh, K. Kobayashi, H. Yamagami, A. Fujimori, A. Tanaka, J. Okabayashi, M. Oshima, S. Ohya, P. N. Hai, and M. Tanaka, Phys. Rev. Lett. **100**, 247202 (2008).

[17] S. Sakamoto, L. D. Anh, P. N. Hai, G. Shibata, Y. Takeda, M. Kobayashi, Y. Takahashi, T. Koide, M. Tanaka, and A. Fujimori, Phys. Rev. B **93**, 035203 (2016).

[18] K. Barmak, J. Kim, L. H. Lewis, K. R. Coffey, M. F. Toney, A. J. Kellock, and J.-U. Thiele, J. Appl. Phys. **98**, 033904 (2005).

[19] C. T. Chen, Y. U. Idzerda, H.-J. Lin, N. V. Smith, G. Meigs, E. Chaban, G. H. Ho, E. Pellegrin, and F. Sette, Phys. Rev. Lett. **75**, 152 (1995).

[20] See Supplemental Material at http://link.aps.org/supplemental/10.1103/PhysRevB.96.144437 for the supercells of L10-(Fe,Co)Pt used in the present calculations.

[21] K. Barmak, J. Kim, L. H. Lewis, K. R. Coffey, M. F. Toney, A. J. Kellock, and J.-U. Thiele, J. Appl. Phys. **95**, 7501 (2004).

[22] I. Galanakis, M. Alouani, and H. Dreyssé, Phys. Rev. B **62**, 6475 (2000).

[23] K. Ikeda, T. Seki, G. Shibata, T. Kadono, K. Ishigami, Y. Takahashi, M. Horio, S. Sakamoto, Y. Nonaka, M. Sakamaki, K. Amemiya, N. Kawamura, M. Suzuki, K. Takanashi, and A. Fujimori, Appl. Phys. Lett. **111**, 142402 (2017).

[24] Y. Nonaka *et al.* (unpublished).

[25] O. Dmitrieva, M. Spasova, C. Antoniak, M. Acet, G. Dumpich, J. Kästner, M. Farle, K. Fauth, U. Wiedwald, H.-G. Boyen, and P. Ziemann, Phys. Rev. B **76**, 064414 (2007).

[26] J. Stöhr and H. König, Phys. Rev. Lett. **75**, 3748 (1995).

[27] In the out-of-plane geometry, where the direction of the light $\vec{k}$ and the applied magnetic field $\vec{H}$ are parallel to the z axis of the lattice or to the surface normal, $7m_T^z/\mu_{\mathrm{B}} \approx -2\Delta n_{z^2} + 2\Delta n_{xy} + 2\Delta n_{x^2-y^2} - \Delta n_{yz} - \Delta n_{xz}$. In the in-plane geometry, where $\vec{k}$, $\vec{H} \parallel \vec{x}$, $7m_T^x/\mu_{\mathrm{B}} \approx \Delta n_{z^2} - \Delta n_{xy} - \Delta n_{x^2-y^2} + 2\Delta n_{yz} - \Delta n_{xz}$ or just $m_T^x = -m_T^z/2$.

[28] I. Galanakis, M. Alouani, and H. Dreyssé, J. Magn. Magn. Mater. **242-245**, 27 (2002).

[29] M. Komelj, C. Ederer, and M. Fähnle, Phys. Rev. B **69**, 132409 (2004).

[30] Because the in-plane orientation of a and b axes are random in our granular films, one could directly compare the in-plane XRD intensity with simulated powder diffraction profile.

[31] E. Yang, D. E. Laughlin, and J. G. Zhu, IEEE Trans. Magn. **48**, 7 (2012).

[32] G. H. O. Daalderop, P. J. Kelly, and M. F. H. Schuurmans, Phys. Rev. B **44**, 12054 (1991).

[33] A. Sakuma, J. Phys. Soc. Jpn. **63**, 3053 (1994).

[34] T. Burkert, O. Eriksson, S. I. Simak, A. V. Ruban, B. Sanyal, L. Nordström, and J. M. Wills, Phys. Rev. B **71**, 134411 (2005).

[35] G. Meyer and J.-U. Thiele, Phys. Rev. B **73**, 214438 (2006).